

# Analyst

Accepted Manuscript



This is an *Accepted Manuscript*, which has been through the Royal Society of Chemistry peer review process and has been accepted for publication.

*Accepted Manuscripts* are published online shortly after acceptance, before technical editing, formatting and proof reading. Using this free service, authors can make their results available to the community, in citable form, before we publish the edited article. We will replace this *Accepted Manuscript* with the edited and formatted *Advance Article* as soon as it is available.

You can find more information about *Accepted Manuscripts* in the [Information for Authors](#).

Please note that technical editing may introduce minor changes to the text and/or graphics, which may alter content. The journal's standard [Terms & Conditions](#) and the [Ethical guidelines](#) still apply. In no event shall the Royal Society of Chemistry be held responsible for any errors or omissions in this *Accepted Manuscript* or any consequences arising from the use of any information it contains.

# Photothermal deflectometry enhanced by total internal reflection enables non-invasive glucose monitoring in human epidermis

M. A. Pleitez<sup>1</sup>, O. Hertzberg<sup>1</sup>, A. Bauer<sup>1</sup>, M. Seeger<sup>1</sup>, T. Lieblein<sup>1</sup>, H. v. Lilienfeld-Toal<sup>2</sup>, and W. Mäntele<sup>1</sup>

<sup>1</sup>Institut für Biophysik, Goethe-Universität Frankfurt, Max-von-Laue-Strasse 1, 60438 Frankfurt am Main, Germany

<sup>2</sup>Elté Sensoric GmbH, 63571 Gelnhausen, Germany

Address for correspondence: [pleitez@biophysik.uni-frankfurt.de](mailto:pleitez@biophysik.uni-frankfurt.de)

## Abstract

We present **TIR-PTD** spectroscopy, an IR-pump/VIS-probe method for the measurement of IR absorption spectra by means of photothermal deflectometry (PTD) enhanced by total internal reflection (TIR). It overcomes the limitations of IR spectroscopy for the study of opaque samples and allows molecular fingerprinting of IR-active liquids or solids. Another important advantage of the presented approach over traditional IR spectroscopy methods is the ability to obtain IR information by means of VIS detection, which is generally much cheaper and easier to handle than IR detection. By application of mid-IR TIR-PTD spectroscopy on human skin *in vivo*, we are demonstrating the correlation between epidermal- and blood-glucose levels on a type 1 diabetic patient.

**Key terms:** Photothermal deflectometry, infrared spectroscopy, quantum cascade laser, total internal reflection, non-invasive glucose measurement.

**Abbreviations:** TIR: total internal reflection; PTD: photothermal deflection; QCL: quantum cascade laser; EC-QCL: external cavity quantum cascade laser; PA: photoacoustic; IRE: internal reflection element; PCA: principal components analysis; PLSR: partial least square regression; IR: infrared; mid-IR: mid infrared; CMOS: complementary metal-oxide-semiconductor; VIS: visible; SNR: signal-to-noise ratio; RMSECV: root mean square error of cross validation; fps: frames per second.

## Introduction

After the absorption of IR light by a sample, the radiationless deexcitation of the vibrational-rotational states produces a temperature increase of the irradiated spot. If the produced heat diffuses to a material in contact with the sample, a temperature gradient resulting in a thermal lens is generated in the coupled material; as seen for instance in the 'mirage-effect' in the air layer next to a sun-exposed street. In the past, several authors have demonstrated that the deflection of a probe beam crossing the optically affected field can be used to study the thermal and optical properties of the sample<sup>1-5</sup>. An IR spectroscopic method based on this principle has unique characteristics unmatched by the traditional IR spectroscopy approaches; like transmission or attenuated total reflectance IR spectroscopy. Perhaps the most remarkable characteristics are its ability to penetrate deep into opaque samples, the capability of performing spectral depth profiling<sup>3,6,7</sup>, its suitability for highly scattering media, and the fact that in this zero-offset technique the measured signal only depends on the amount of absorbed light; characteristics shared by most of the photothermal- and photoacoustic-based spectroscopic methods<sup>8-12</sup>. However, the realization of such a spectroscopic technique for the analysis of biological samples, especially *in vivo*, has been limited in part by the weak interaction of the probe beam with the thermal field in the coupling media, and by the complicated optical adjustment requirements between sample, excitation beam, and probe beam. Besides, another limiting factor has been the lack of strong and tunable laser sources in the mid-IR.

We addressed these limitations and were able to enhance the 'mirage-effect' by guiding the probe beam directly to the photothermally produced heat source by means of total internal reflection (TIR). This was done using an internal reflection element (IRE) as probe beam guidance also acting as the coupling material. As excitation source we used an external cavity quantum cascade laser (EC-QCL) emitting mid-IR radiation. We were able to demonstrate the potential of the proposed method for the analysis of biofluids or any other IR-active liquid or solid sample. As a promising biomedical application, we could demonstrate the correlation of blood glucose with glucose levels in the epidermis of a type 1 diabetic patient. This IR sensor principle could therefore be the basis for non-invasive glucose measurement for diabetes patients.

## Results and discussions

### Working principle of the TIR-PTD spectrometer

The key components of the TIR-PTD spectrometer are the pump laser, the probe laser, and the internal reflection element (Fig. 1a&b). As pump laser we used an EC-QCL tunable from 1000  $\text{cm}^{-1}$  to 1245  $\text{cm}^{-1}$ . This light source has an average power output of 7.5 mW max. for a duty cycle of 5% and a pulse repetition rate ranging from 100 Hz to 100 kHz; for all experiments we used the maximum pulse width of 500 ns. The probe beam is emitted by a laser diode with 5 mW power output at 655 nm and a Gaussian beam intensity profile. The IRE is a truncated

1  
2  
3 right-angle prism (Dove prism) made out of a ZnS crystal cut in such a way that the sloped  
4 edges form an angle of  $45^\circ$  with the base. The angle of incidence of the probe beam to the  
5 sloped edge of the IRE is adjusted in order to produce total internal reflection at the surface  
6 directly below the sample/IRE interface. The pump beam is normal to the truncated base of the  
7 prism and it is focused to the spot where the internal reflection of the probe beam is located.  
8  
9 The IRE used here has a high transmittance, about 70%, for the pump and the probe beam and  
10 it is thus considered 'transparent' for both laser beams. With this configuration, the pump beam  
11 is adjusted to irradiate the sample at exactly the spot of total internal reflection of the probe  
12 beam. The absorption of IR light by the sample and its radiationless relaxation produces a local  
13 increase of temperature, which generates a thermal lens in the IRE that deflects the probe  
14 beam along the vertical and horizontal direction (Figs. 2a-c). Since the triggering effect is the  
15 photothermal deposition of energy in the sample, the intensity of the probe beam deflection, *i.e.*  
16 the deflection angle, depends directly on the output power of the pump laser and on the  
17 absorption coefficient of the sample (Fig. 2d & Figs. 3A-d); no significant variations in the  
18 intensity of the probe beam due to temperature-related changes of its penetration depth in the  
19 sample were observed. This photothermal beam deflection is at least  $10^6$  higher than the  
20 deflection caused by the photoacoustic pressure wave and the Goos-Hänchen displacement  
21 and, therefore, both can be neglected<sup>13-15</sup>. By modulating the pump beam, the temperature at  
22 the sample/IRE interface and, consequently, the deflection of the probe beam oscillates with the  
23 same frequency of the thermal lens generated in the IRE by the sample's IR absorption (Fig.  
24 2e). The latter is the very basic sensing signal for spectroscopy in the presented approach; the  
25 amplitude of the modulated deflection of the probe beam measured by a position sensitive  
26 quadrant diode detector. The absorption spectrum of a given sample is obtained by recording  
27 the output signal of a lock-in amplifier for different wavelengths along the emission range of the  
28 EC-QCL (Fig. 1b).

### 43 ***In vitro* and *in vivo* TIR-PTD spectroscopy of glucose**

44 The absorption spectra of aqueous glucose solutions measured by TIR-PTD exhibit, as  
45 expected, the well-known spectral features of the glucose molecule in the fingerprint region<sup>16</sup>  
46 (Figs. 3a&c). These spectra were obtained with a signal-to-noise ratio (SNR) between 140 and  
47 300, defined as the inverse of the relative standard deviation; meaning that changes as small as  
48 0.3% in the spectral features of a given sample can be detected. The TIR-PTD signal shows a  
49 broad linear response with the increase of glucose concentration in the whole range between 0  
50 and 5000 mg/dL (Figs. 3b&d). The glucose concentration range from 20 to 400 mg/dL is of  
51 special interest for a future application in non-invasive glucose monitoring. In this concentration  
52 range for glucose *in vitro*, an error of prediction of 7.6 mg/dL was found by partial least square  
53 regression.

54  
55  
56  
57  
58  
59  
60 Additional to the *in vitro* measurements, the TIR-PTD spectra of a post-pandrial type 1 diabetic

1  
2  
3  
4  
5  
6  
7  
8  
9  
10  
11  
12  
13  
14  
15  
16  
17  
18  
19  
20  
21  
22  
23  
24  
25  
26  
27  
28  
29  
30  
31  
32  
33  
34  
35  
36  
37  
38  
39  
40  
41  
42  
43  
44  
45  
46  
47  
48  
49  
50  
51  
52  
53  
54  
55  
56  
57  
58  
59  
60

volunteer was measured for 1 hour (one laser-scan every 6 seconds) after insulin administration. During this time, the glucose concentration in blood, measured by a standard enzymatic device, dropped from 188 to 91 mg/dL. In general, the mid-IR spectrum of skin in the fingerprint region is dominated by the  $\text{PO}_2^-$  vibrations (symmetric stretch at  $1080\text{ cm}^{-1}$  and antisymmetric stretch at  $1240\text{ cm}^{-1}$ ), C-O, C-O-C and C=O vibrations ( $1047\text{ cm}^{-1}$ ,  $1120\text{ cm}^{-1}$ ,  $1159\text{ cm}^{-1}$  respectively). These spectral features are mainly explained by the dominant content of lipids and proteins in skin, in particular, keratin from the *Stratum corneum*<sup>17,18</sup>. Since the mid-IR spectrum of glucose exhibits the specificity of a molecular fingerprint, it can be detected among the many other IR-active biomolecules in human skin by means of principal component analysis (PCA). Both, the scores of PC2 as well as its loadings fit to the spectral features of glucose *in vitro* and to the time course of the glucose concentration in blood, respectively (Figs. 4a&b). With this spectral information it was possible to establish a calibration system by means of PLS-regression. With a prediction error of 9 mg/dL, the leave-one-out cross-validation of this calibration system shows that the glucose concentration in human epidermis correlates well with the glucose concentration in blood (Figs. 4c&d).

## Conclusions

In summary, TIR-PDT make it possible to measure IR absorption spectra of opaque samples at penetration depths for the pump beam only limited by the absorption coefficient and the thermal diffusion length of the sample. Applied to skin, it allows to reach the glucose-containing interstitial fluid in the *Stratum spinosum* in order to monitor the glucose levels non-invasively and *in vivo*. By means of TIR-PTD we can obtain spectral information from much deeper layers than what is possible with established IR methods like, for instance, attenuated total reflectance IR spectroscopy. The penetration depth for the latter is around 2 - 4  $\mu\text{m}$  in skin, depending on the wavelength of the excitation beam and the refractive index of the IRE.

Since TIR-PTD is based on the photothermal effect, a depth profiling of the absorption and an analysis of the thermal properties of the samples is possible using different modulation frequencies. The latter opens the possibility of applying the presented setup in some previously reported photothermal-based imaging techniques<sup>6,7</sup> as well as in the analysis of skin properties or biofluids. An additional advantage of this technique is the ability of getting IR information by VIS detection; VIS optics and detectors are generally much cheaper and easier to handle than IR systems.

## Material and methods

### General description of the TIR-PTD spectrometer

The probe beam emitted by a laser diode (Edmund Optics Modell-No. 57-108) with an average power of 5 mW at 655 nm is focused into the IRE to form a spot with a diameter below 100  $\mu\text{m}$  at the interface between the IRE and the sample. After leaving the IRE the probe beam passes

1  
2  
3 an iris (17 cm behind) to block some stray light and to ensure a clear spot with a maximum size  
4 of 1.5 mm at the detector. The vertical deflection of the probe beam was measured using a  
5 position-sensitive quadrant photodiode detector (Thorlabs, PDQ80A) located at 18 cm from the  
6 irradiated spot. This sensor has a diameter of 7.8 mm, a rise time of 40 ns, and it is sensitive  
7 between 400-1050 nm. The modulated signal measured by this detector was filtered and  
8 amplified by a lock-in amplifier (SR810, Stanford Research Systems) using a time constant of  
9 100 ms. The pulsed pump beam, focused to form a spot of about 300  $\mu\text{m}$  at the IRE/sample  
10 interface, was further modulated by a mechanical chopper (ThorLabs MC 2000) at a frequency  
11 of 63 Hz. The thermal diffusion length of the thermal wave thus produced is approximately 30  
12  $\mu\text{m}$  in water<sup>6</sup>. At this frequency, which served as reference for the lock-in amplifier, the  
13 measured spectra yielded the highest SNR and the most stable modulation. The output signal of  
14 the lock-in was digitized by a data acquisition card (NI 9239, National Instruments) and stored  
15 on a personal computer controlled by LabView (10.0f2, National Instruments) for further  
16 processing with MatLab (v. 7.1.0.246 (R14), Mathworks) and the PLS-toolbox (v. 4.01,  
17 Eigenvektor) (Fig. 1b).

### 27 **System characterization**

28  
29 For the characterization and visualization of the photothermal effect and the resulting probe  
30 beam deflection, intensity profiles of the probe beam at On/Off pump beam were recorded. For  
31 these experiments, four detection distances along the probe beam propagation were selected  
32 (46, 61, 76, and 91 cm) having the excitation spot as starting point. For detection, a C-mount  
33 microscope camera (ToupTek, UCMOS05100KPA-MT9P001) equipped with a 5.1 megapixel  
34 CMOS sensor (Aptina MT9P001) containing a pixel size of 2.2 x 2.2  $\mu\text{m}$  was used. With this  
35 system, we generated an image stack of a 60 second recording window with a rate of nearly 60  
36 fps and a resolution of 640 x 480 pixel. To avoid saturation of the sensor, the exposure time was  
37 adapted in the range between 5 and 10 ms and a 5% neutral density filter was placed in the  
38 light pathway. Using ImageJ 1.48q, the recorded image stack was transferred into an intensity  
39 map containing averaged and normalized intensity values for each pixel. Prior to analysis, a  
40 two-dimensional convolution kernel filter handling a 10 x 10 pixel area of the intensity map was  
41 used as a post-processing step to smooth out the raw data (MatLab 7.1.0.246 (R14),  
42 Mathworks).

52  
53 Linearity between QCL output power and the probe beam deflection was verified by measuring  
54 the TIR-PTD signal of a water sample irradiated at 1170  $\text{cm}^{-1}$  with a fixed chopper frequency (63  
55 Hz) and with different QCL pulse repetition rates; from 50 to 100 kHz in steps of 2 kHz.

57 For the spectroscopic measurements, the wavelength of the pump beam was scanned across  
58 the whole emission range of the EC-QCL; one scan takes about six seconds. In order to  
59 increase the SNR of the spectra, multiple scans were averaged: 20 scans for the sample and 50  
60 scans for the reference; a 25  $\mu\text{L}$  drop of water. The actual spectra were calculated by dividing

1  
2  
3 the average of the sample scans by the average of the reference scans.  
4

### 5 **Spectroscopic measurement and chemometric methods**

6  
7 In order to estimate the sensitivity of TIR-PTD to detect changes in the concentration of an  
8 analyte in a simple matrix, *i.e.* water, two series of aqueous glucose concentrations were  
9 measured (sample volume 25  $\mu\text{L}$ ). The first series had a glucose concentration from 500 mg/dL  
10 to 5000 mg/dL. The spectra measured for this series were normalized by dividing the TIR-PTD  
11 signal at each wavenumber by the signal at 1184  $\text{cm}^{-1}$ . This wavenumber was selected for  
12 normalization because here glucose shows the lowest absorption in the considered spectral  
13 range. The second series of glucose spectra, with concentrations in the physiological range,  
14 was measured from 0 mg/dL to 400 mg/dL in steps of 40 mg/dL. These spectra were analyzed  
15 using two chemometric methods: *principal component analysis* (PCA) and *partial least square*  
16 *regression* (PLSR). PCA iteratively decomposes the spectral data into principal components  
17 (PC) each representing the maximum remaining variance. Every PC is composed of a *scores*  
18 and a *loadings* vector which represent the PC's spectra and concentration, respectively<sup>19</sup>.  
19

20 For prediction of the glucose concentration from the TIR-PTD spectra, a PLSR was performed.  
21 This method is an extension of multiple linear regression that is capable of quantitatively  
22 analyzing data that are both noisy and collinear<sup>20</sup>. Instead of directly modeling the dependent  
23 data, PLSR calculates latent variables that are then used to estimate the dependent data.  
24 Similar to the principal components of PCA, these latent variables model the variance and are  
25 orthogonal to each other<sup>21</sup>. However, they additionally have to correlate with the dependent  
26 variables. This third condition makes them different from the principal components of PCA and  
27 enables quantitative prediction.  
28

29 Continuous TIR-PTD spectra were measured *in vivo* on the left hypothenar of a type 1 diabetic  
30 volunteer. A set of 400 scans (resulting in 20 spectra) were recorded over 70 minutes during the  
31 correction of postprandial glucose values with insulin. Parallel to TIR-PTD spectroscopy, every  
32 five minutes the blood glucose concentration was measured by a clinical blood glucometer  
33 (Hemocue B glucose analyzer, Hemocue) with a precision of  $\pm 4.3$  mg/dL. The resulting spectra  
34 were processed by PLSR and PCA. In order to avoid over-fitting, in the PLSR model, the  
35 number of latent variables was determined by the minimum RMSECV<sup>20</sup>.  
36  
37  
38  
39

### 40 **Acknowledgements**

41 The authors would like to thank Ernst Winter, Institut für Biophysik Goethe-Universität, for  
42 excellent mechanical engineering. Dr. Andreas Roth and Dr. Georg Wille are gratefully  
43 acknowledged for valuable discussions on electronics and biochemical aspects, respectively.  
44 Arne Küderle, a student in our group is acknowledged for his help with the measurements.  
45  
46  
47  
48  
49  
50  
51  
52  
53  
54  
55  
56  
57  
58  
59  
60

**Bibliography**

1. N. A. George, *Appl. Phys. B Lasers Opt.*, 2003, **77**, 77–80.
2. A. C. Boccara, D. Fournier, and J. Badoz, *Appl. Phys. Lett.*, 1980, **36**, 130.
3. W. B. Jackson, N. M. Amer, A. C. Boccara, and D. Fournier, *Appl. Opt.*, 1981, **20**, 1333–44.
4. R. M. Banish, R.-F. Xiao, and F. Rosenberger, *J. Appl. Phys.*, 1988, **64**, 2907.
5. M. Pfeifer, A. Ruf, and P. Fischer, *Opt. Express*, 2013, **21**, 25643.
6. J. Opsal, *J. Appl. Phys.*, 1982, **53**, 4240.
7. A. Rosencwaig, *J. Appl. Phys.*, 1980, **51**, 2210.
8. D. V Bageshwar, A. S. Pawar, V. V Khanvilkar, and V. J. Kadam, *Eurasian J. Anal. Chem.*, 2010, **5**, 187–203.
9. C. Haisch, *Meas. Sci. Technol.*, 2012, **23**, 012001.
10. C. S. Sunandana, *Phys. status solidi A*, 1988, **105**, 11–43.
11. A. Rosencwaig, *Adv. Electron. Electron Phys.*, 1978, **46**, 207–311.
12. J. M. Rey, J. Kottman, and M. W. Sigrist, *Appl. Phys. B*, 2013, **112**, 547–551.
13. J. C. Murphy and L. C. Aamodt, *J. Appl. Phys.*, 1980, **51**, 4580.
14. C.-F. Li, *Phys. Rev. A*, 2007, **76**, 013811.
15. R. Yang, W. Zhu, and J. Li, *Opt. Express*, 2014, **22**, 2043.
16. L. P. Kuhn, *Anal. Chem.*, 1950, **22**, 276–283.
17. D. T. Downing, *J. Lipid Res.*, 1992, **33**, 301.
18. P. Garidel, *Phys. Chem. Chem. Phys.*, 2002, **4**, 5671–5677.
19. S. Wold, K. Esbensen, and P. Geladi, *Chemom. Intell. Lab. Syst.*, 1987, **2**, 37–52.
20. S. Wold and M. Sjostrom, *Chemom. Intell. Lab. Syst.*, 2001, **58**, 109–130.
21. W. G. Glen, W. J. D. Ih, and D. R. Scott, *Tetrahedron Comput. Methodol.*, 1989, **2**.



## Figures

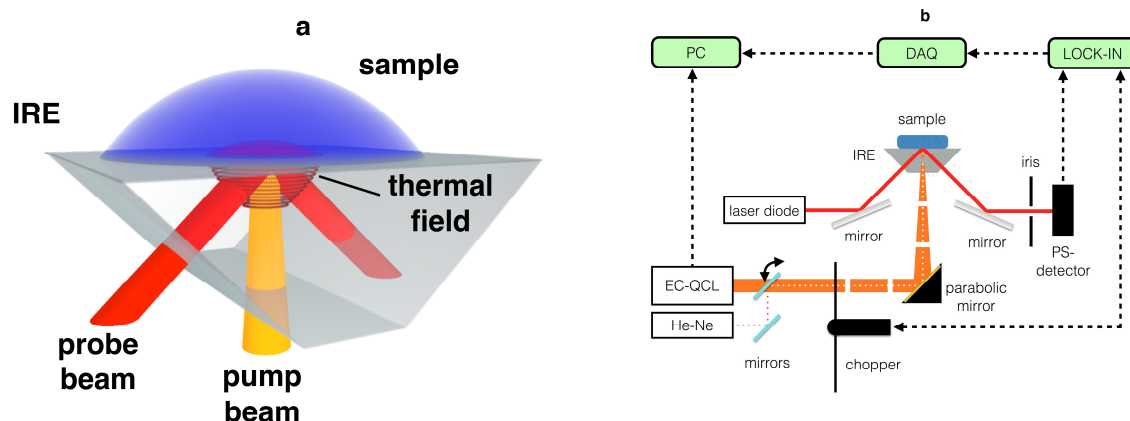
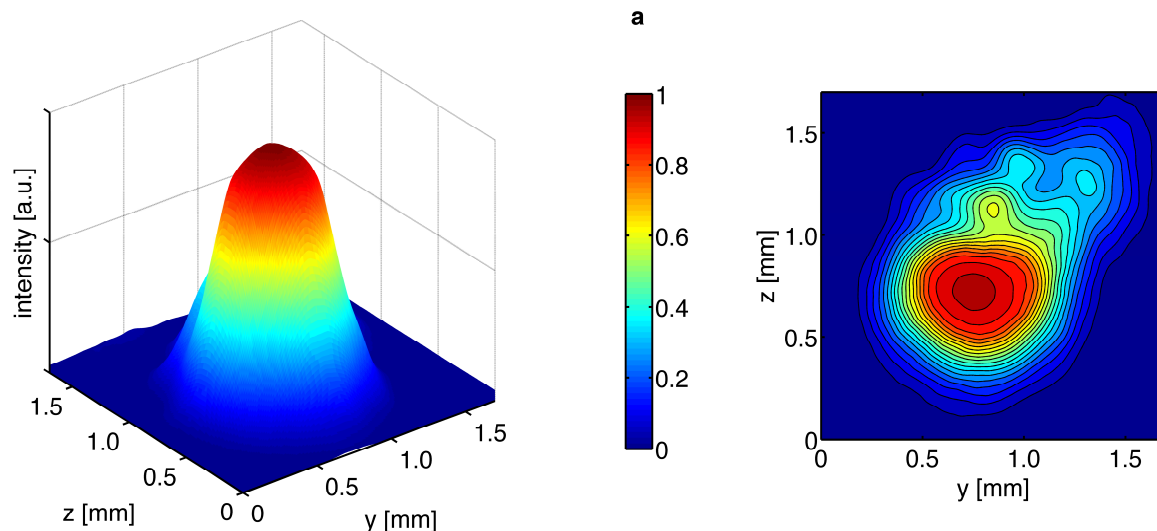
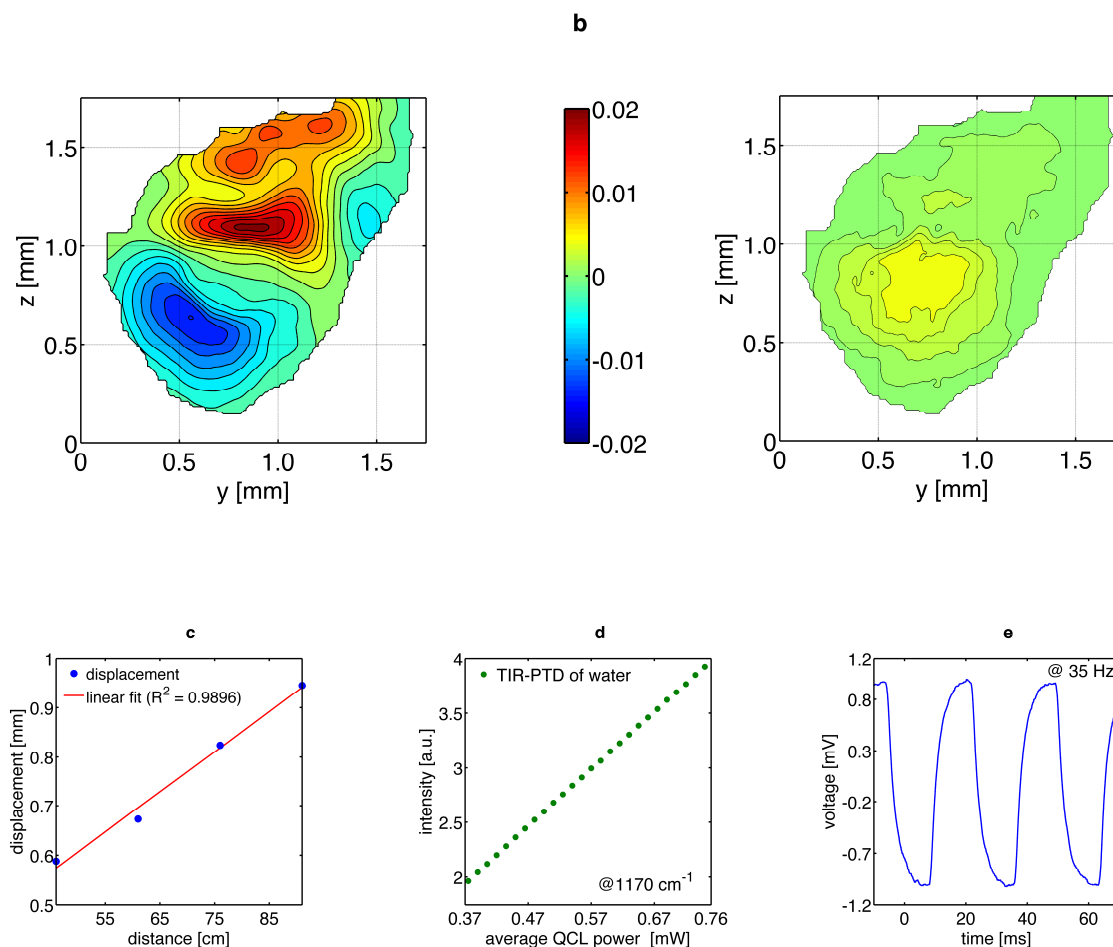


Figure 1:

(a) Principle of the TIR-PTD spectrometer as filed for patent under DE 10 2014 108 424.1

(b) The tunable pulsed QCL is modulated by the chopper and serves as pump laser to irradiate the sample and to produce a thermal field due to IR absorption. This thermal field couples into the IRE where the probe beam from the red laser diode is totally reflected. The irradiation spots of the pump and probe beam spatially overlap. A refractive index change is induced due to the thermal field, resulting in the deflection of the probe beam. This deflection is measured by an intensity change on a position sensitive photodiode detector. An iris aperture is used to block stray light. The signal at the photodiode is amplified, filtered by a lock-in amplifier and stored on a computer for further processing.





**Figure 2: Characterization of the beam displacement:**

(a) 3D surface (left) and contour plot (right) of the intensity profile of the probe beam detected by a CMOS sensor (distance from IRE: 46 cm).

(b) Beam displacement on the CMOS Sensor due to deflection in the IRE. The undeflected beam profile was subtracted from the deflected beam profile.

left: Intensity differences for a water sample with and without IR-excitation. QCL repetition frequency 100 kHz at 1170 cm<sup>-1</sup>

right: Control with IR-pump beam blocked. The same result is obtained if no sample is located atop of the IRE (data not shown)

(c) Linear dependence of the CMOS sensor signal with varying detecting distance.

(d) TIR-PTD signal of water at 1170 cm<sup>-1</sup> vs. QCL power, adjusted by the pulse repetition rate.

(e) Detector signal transient representing the rise and decay of temperature indicated by deflection. The rise and decay time of the signal are specific for the heat capacity and conduction of the sample and the IRE.

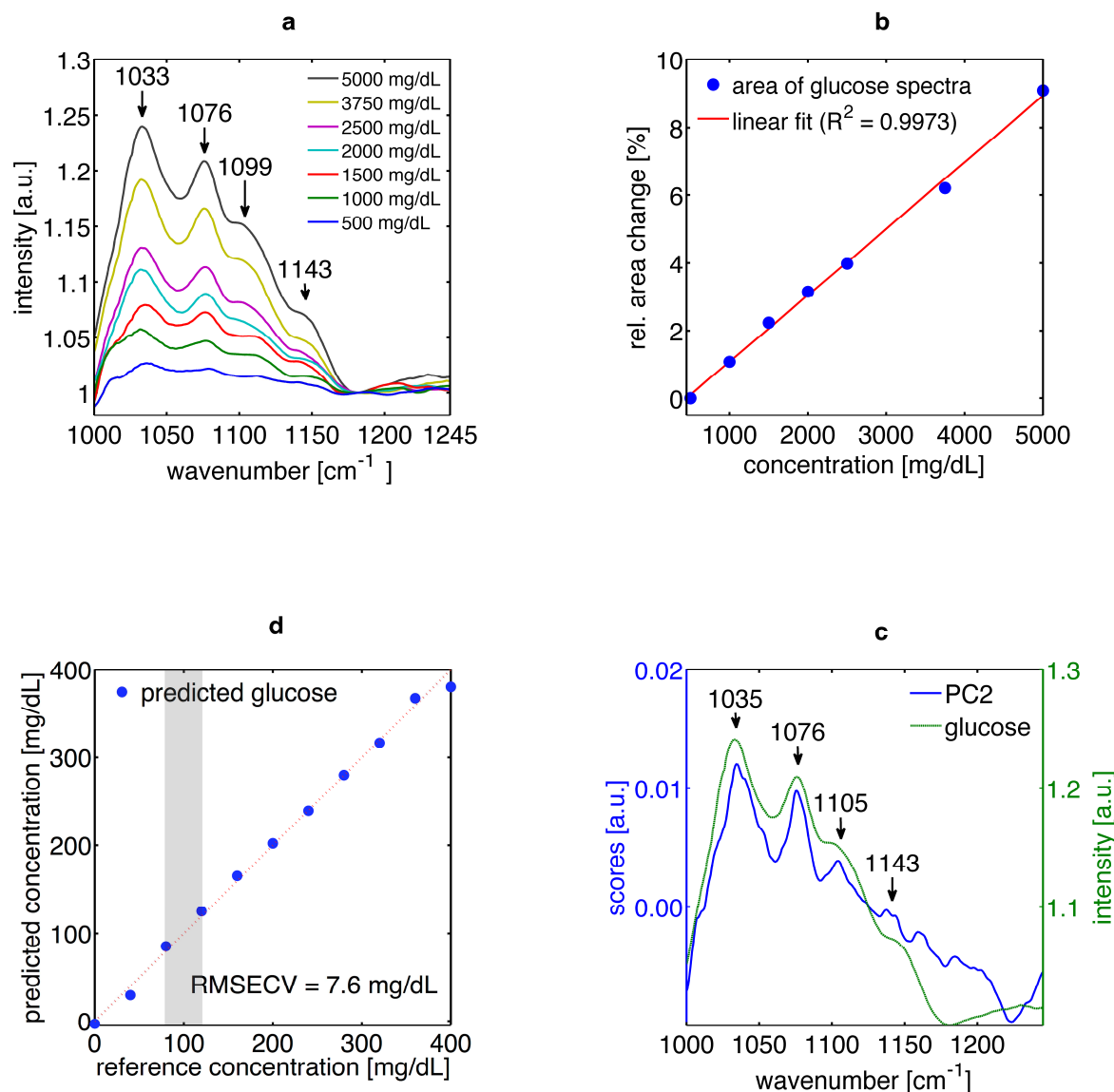


**Figure 3: *In vitro* measurements on aqueous glucose solutions:**

(a) TIR-PTD spectra of glucose solutions in the range of 500 to 5000 mg/dL; glucose is identified by its characteristic peaks.

(b) Integrated absorption vs. glucose concentration. The integrated absorbance between 1015 and 1245  $\text{cm}^{-1}$  correlates linearly with the glucose concentration with a regression coefficient of 0.9973.

(c) Solid line: principle component 2 (PC2) of the spectra for physiological glucose concentrations (0 to 400 mg/dL).

Dashed line: spectrum at high glucose concentration (5000 mg/dL) as shown in (a) demonstrating that glucose can be detected with chemometric tools at lower concentrations.

(d) PLSR cross validation for spectra of the physiological glucose concentrations, the shaded area indicates the normal glucose concentration range on a healthy person (80 - 120 mg/dL).

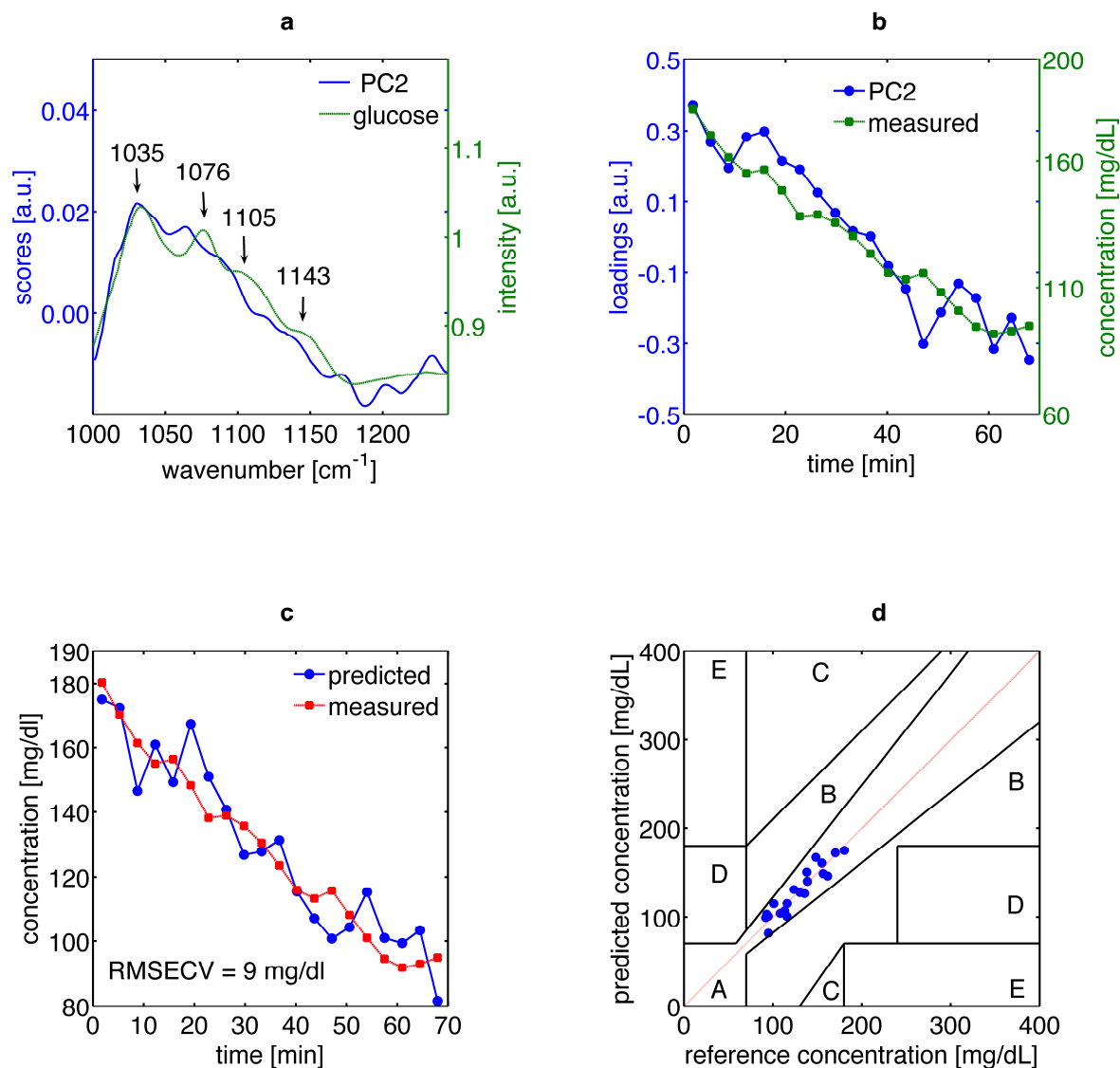


**Figure 4: *In vivo* measurements on a volunteer:**

(a) Solid line: principle component 2 (PC2) of the skin spectra.

Dashed line: spectrum at high glucose concentration (5000 mg/dL) as shown in 3(a).

In general, the scores of PC2 represent most of the spectral features of glucose. However, as seen for the absorption band at 1076 cm<sup>-1</sup>, some mismatches are expected because of the comparison of glucose measured in different media; skin and water solutions. Besides, the scores of PC2 might show the linear combination of other components in the matrix.

(b) Solid line: time course of loadings of PC2

Dashed line: time course of invasively measured blood glucose concentration during the test.

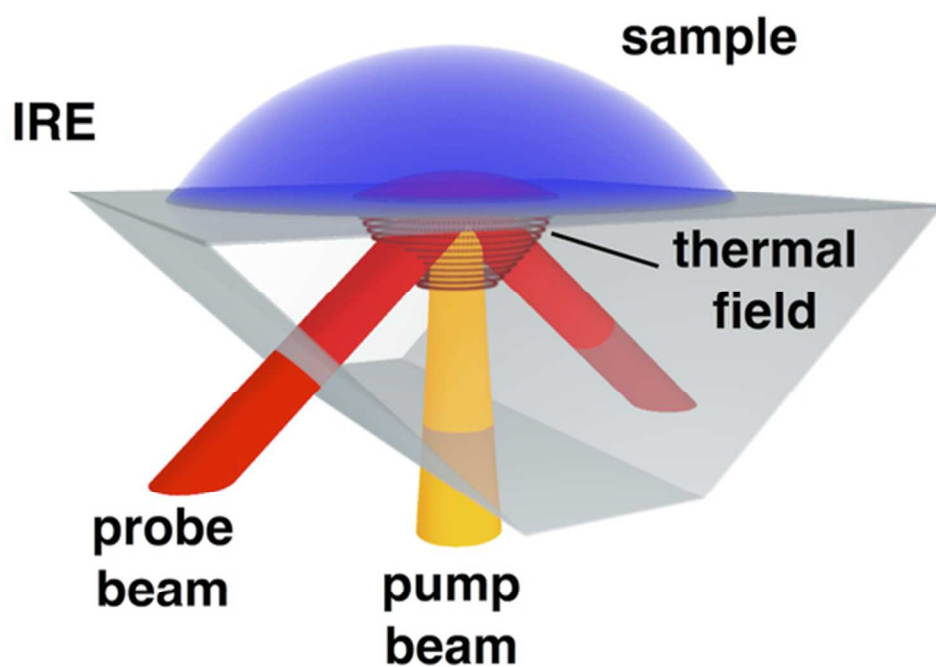
(c) Cross-Validation of the partial least square regression.

Dashed line: time course of blood glucose measured invasively.

Solid line: non-invasively measured glucose level in the interstitial fluid, as calculated by PLSR, follows without delay the invasively measured blood glucose values.

(d) Clarke error grid for the PLSR with 100% of predicted values in zone A (required for clinical

1  
2 applications).  
3  
4  
5  
6  
7  
8  
9  
10  
11  
12  
13  
14  
15  
16  
17  
18  
19  
20  
21  
22  
23  
24  
25  
26  
27  
28  
29  
30  
31  
32  
33  
34  
35  
36  
37  
38  
39  
40  
41  
42  
43  
44  
45  
46  
47  
48  
49  
50  
51  
52  
53  
54  
55  
56  
57  
58  
59  
60



We present an IR-pump/VIS-probe method for the measurement of IR absorption spectra by means of photothermal deflectometry (PTD) enhanced by total internal reflection (TIR). This technique is termed TIR-PTD spectroscopy.  
51x35mm (300 x 300 DPI)